Chapter 7

EXPERIMENTS ON SALINITY INFLUENCE

Bubbles have been under investigation for a long time as the brief summary on physical findings (Chapter 2) and the review of previous studies (Chapter 3) show. Fluid dynamics researchers have done a lot of modeling and theoretical considerations about the bubble drag, bubble rise velocity, bubble volume oscillation etc. Those were confirmed or refined by a set of precise and comprehensive experiments (Clift et al., 1978; Brennen, 1995) . On the other hand, chemists have investigated thoroughly the interfacial effects for different surface active materials, which is a necessary knowledge for bubble studies as bubbles represent many interfaces in the bulk of fluid (Rosen, 1978; Adamson, 1982) . Finally, the physical oceanographers are interested how the sea water composition, in particular its major ionic constituents sodium (Na) and chloride (Cl), influence the bubbles' physical behavior (§§2.7 and 3.6.4) . However, often the results obtained within one of these three communities stay confined to that community. Moreover, these results are usually for a single, isolated

bubble. It would be helpful to apply the fluid dynamics and chemistry knowledge to oceanography to understand better the bubble behavior in sea water. In addition, as in the real ocean clouds of bubbles produced by breaking waves are constantly overlapped on the background bubbles population it is of interest and necessity to observe the bubble cloud characteristics and behavior in salt water.

Motivated by this need, experiments on salinity influence on bubbles and bubble clouds characteristics were conducted. Quantitative result was sought on the question does (and how) a range of salinities alter the cloud shape and penetration depth, and the number of bubbles within the cloud. The fundamental interest what is the effect of salt, other influences excluded, on the characteristics of an individual bubble justified the conducting of experiments on a single bubble with a controlled size. In particular, possible changes of the bubble diameter, d, rise velocity, V_r, and surface lifetime, t, were of interest.

7.1 Experimental Equipment

Several experiments were performed in two stages. To begin, the characteristics of a single bubble were observed at different salinities in three experiments. Then the influence of the salt on bubble clouds was investigated. The measurements included direct observations and observations from video records.

In both cases the experiments were performed in transparent tanks. Single bubbles were generated by forcing atmospheric air through a capillary tube. Tubes of

various inner diameter were used for the different experiments. Bubble clouds were simulated with a water jet.

The video records were made with standard (30 fps) cameras. For the single bubble experiments cameras Panasonic AG-160 and Panasonic WV-3400 were employed: one for recording the bubble rise to the surface from a side view, another for bubble lifetime on the surface from a top view. The bubble clouds were documented with the Burle camera. Descriptions of both of these (Panasonic AG-160 and Burle) are given in §6.1.2. The Panasonic WV-3400 has a set of lenses from 12.5 to 75 mm providing zoom 6 times and minimum required scene illumination of 50 lx. The camera has no shutter speed, but has an electronic timer with an accuracy of 1/100 s. These features made it the best choice for bubble surface lifetime video records. Front lighting with two 600-W lamps made the bubbles to appear in the video records as bright spots. The visualization of those was further improved by locating dark screens on the back tank wall and beneath the tank. Images of bubbles and bubble clouds were digitized from the video records with the frame grabber 4MEG VIDEO and processed with the interactive image processing software 4MIP (Epix Inc.), both described in detail in §6.1.3.

The parameters necessary to be controlled during the experiments were flow rate, salinity, surface tension and temperature. The salinity was measured with a salinometer based on a light refraction principle (Aquatic Eco-Systems, Inc.) . The tensiometer used (Biolar Corp.) is based on Wilhelmy slide method, whose principle is well described by Adamson (1982) . A thin plate of platinum foil, which weight is

preliminary balanced with a Roller-Smith precision balance, is lowered gradually toward the measured liquid sample until it just touches the surface. The surface tension then pulls down the plate and the increase in the weight is noted. The weight change reading, in mg, is multiplied with a coefficient specific for the instrument (0.1909), and the surface tension is obtained in dynes cm^{-1} (= mN m^{-1}) . The water temperature was regularly read with a thermistor thermometer (Cole-Parmer Instrument Company) .

7.2 Experimental Conditions

7.2.1 Single Bubble

Three different experiments were performed for studying the single bubble characteristics at various salinities. The first two experiments were conducted in a tank with sizes 121.9 cm L x 32.4 cm W x 39.0 cm H, with a water depth of 32.4 cm. The tap water used was filtered by two mechanical filters of sizes 5 and 1 μm and a charcoal canister. With these dimensions the experimental volume was 0.128 m^3, or mass of 127.1065 kg.

The dissolving of salt in such a big volume required some time. This, however, was critical for forming of a dense surface active film, which altered undesirably the parameters measured, especially the surface lifetime. Also, there was some organic contamination in the water even after the filtering. Those reasons, together with the aim to investigate the pure effect of salt, led to the decision the third experiment to be conducted with distilled water and in a smaller tank with sizes of 30.2 cm L x 30.3

cm W x 27.8 cm H with a water depth of 26.5 cm; experimental volume of 0.024 m^3, or mass of 24.25 kg. Though small, the tank dimensions relative to the bubble size were enough large to avoid wall effects.

In all three experiments bubbles were generated by forcing atmospheric air through a capillary. The diameter of the capillary orifice determined the size of the bubble generated. For the first two experiments (in a big tank with a filtered water) a capillary with an inner diameter, 2R, of 1.5 mm was used. In the third experiment (in a smaller tank with a distilled water) capillaries with three different inner diameters were employed: those were about 0.5, 1 and 1.15 mm. Using the formula relating the bubble size to the capillary orifice radius at 20^{o}C, $R = 9.05r^3$ (see § 2.2.2), it is possible to predict the sizes of the bubbles produced, d_{pred}, and they are listed in the Table 7.1. Note that, though the values for 2R in the table are reported in mm, the calculations in $R=9.05r^3$ must be in cm as the parameters inthe constant 9.05 use cm.

Table 7.1

Capillary inner diameter, 2R (mm)	1.15	1	0.5
Predicted bubble diameter, d_{pred} (mm)	3.7	3.54	2.81
Flow rate, F (cm^3 min^{-1})	0.53	0.464	0.232

In choosing the capillary diameters, hence the size of the bubbles generated, the reliability of observation and video system resolution rather than the direct oceanographic relevance were leading concerns, as the general effect of salt on bubbles was under investigation. The expected bubble sizes point that the parameters measured

should follow the principles of the intermediate region (§ 2.2.3 and 2.3.3): ellipsoidal bubbles moving upward on a zigzag path with a velocity decreasing with bubble size increasing.

During the direct observations an electronic stopwatch was used to measure: 1) the time necessary for a bubble to travel along a reference distance from the moment of its formation at the capillary orifice to its surfacing; 2) the time from the moment of bubble appearance on the water surface to its bursting. Up to 15 readings for both times were taken. The video record duration for the different experiments ranged from 2 to 4 minutes. A ruler located in the camera's side field of view yielded the reference traveling distance.

7.2.2 Bubble Clouds

One experiment was performed for studying the bubble cloud characteristics at various salinities. Bubble clouds were generated by a water jet coming out from a tube with an inner diameter of 4.44 mm under angle of 45^{o} and at a distance of 9.5 cm from the water surface (Figure 7.1) . This idea, proposed by Koga (1982), provides a good simulation of bubble production by breaking wave in a small tank. The effect of the inclination angle on the bubble clouds generated was investigated first by Koga (1982) and more systematically by Detsch and Sharma (1990) . Bubbles are not generated beyond some critical angle, which varies with the tube inner diameter and the injection velocity. According to their results, with the size of the tube reported here and the impact jet velocity (given below) an inclination angle of 45° is in the middle of the

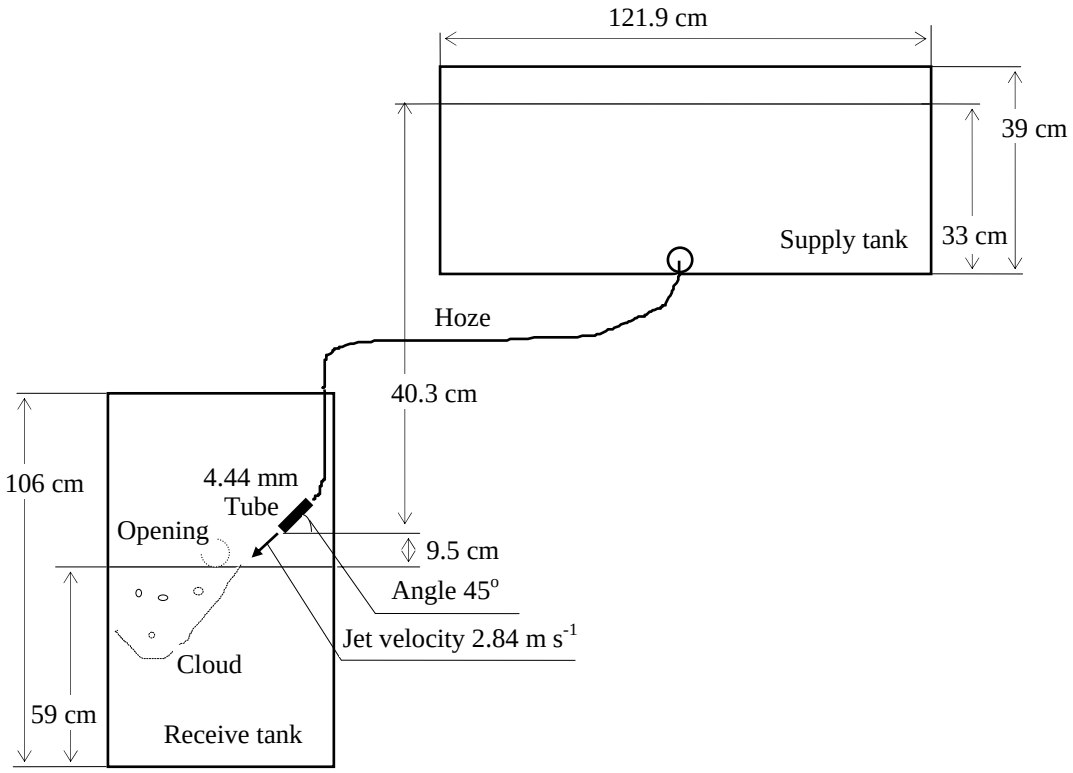

Figure 7.1 Schematic of the experimental setup for bubble clouds.

range of possible angles, and far from a critical angle. Hence, uncertainties from a proximity to the critical inclination angle are eliminated. The water jet was furnished to a "receiving" tank, where the clouds were formed, from a "supply" tank by a hose. The supply tank was with sizes of 121.9 cm L x 32.4 cm W x 39.0 cm H and a water depth of 33 cm, which presented a volume of 0.13033 m^3, or a mass of 130.33 kg. The receiving tank had sizes of 39.5 cm L x 39.5 cm W x 106 cm H with a water depth of 59 cm, which gave a volume of 0.09205 m^3, or a mass of 92 kg. The height difference, h, between the water level in the supply tank and the end of the tube producing the jet was 40.3 cm which

gave a value of the impact speed of the jet, V = 2.84 m s^{-1}; the calculation uses the Bernoulli's equation, $V = (2gh)^{½}$. The huge amount of water in the supply tank assured that this speed remained roughly constant for the time necessary to make the video records (about 1 min) . The water level in the receiving tank was at the lower rim of a circular opening on one of the side wall at a height of 61 cm from the bottom. When the jet was falling into the receiving tank and producing bubble clouds, the excess of water ran out from this opening into a clean bucket. In this way the water level in the receiving tank was maintained constant. The excessive amount of water, collected in the bucket, was returned back in the supply tank after the measurement in order to start the next one at all the same water levels. The water used in both, receiving and supply, tanks was filtered.

Bubble clouds were recorded for 1 minute. Standard video camera, Burle, was used with a focus length of 12.5 mm, aperture 5.6, and shutter speed 1 ms. The camera looked at the clouds in a side view, perpendicular to the tank wall and below the water level. With a working distance of 27.5 cm from the tank the horizontal and vertical scales were 0.296 mm pxl^{-1} and 0.698 mm pxl^{-1}, respectively. Thus, the sensitive area of the camera (768 pxl x 494 pxl) viewed on a field of 22.7 cm x 17.25 cm.

7.2.3 Controlled Parameters

The parameters salinity, S ($^{o}/_{oo}$), surface tension, γ (mN m^{-1}), water temperature, T (°C), and flow rate, F (cm^3 min^{-1}) were controlled during the experiments.

The influence of the flow rate on bubble rise velocity could not be avoided completely (see §2.2.2) . Thus, the air pressure, furnished to the capillary, was controlled with a fine valve to be constant for all measurements: 10 bubbles for 30 seconds. With the predicted diameters this bubble production would give flow rate values, F in $cm^3\ min^{-1}$ (listed in Table 7.1), which are low enough to keep the bubble sizes independent of F (see also Figure 2.2) . In addition, whatever initial speed the bubbles received from the air flow, it was minimized by the horizontal orientation of the capillary.

The salinity of the water in all experiments was changed by adding an appropriate amount of salt (NaCl) to a given volume of water in order to increase the saltiness in a step of roughly 4 - $6^o/_{oo}$. For example, in the first two experiments on a single bubble (water mass of 127.1065 kg) the calculations showed that by adding 600 g salt to this water mass would change the salinity with a step of $4.7^o/_{oo}$ (4.7 g kg^{-1}) . The salinity range covered, from fresh water (ideally $0^o/_{oo}$) to about $40^o/_{oo}$, was chosen to be oceanographically relevant, including values in estuaries and in the open ocean. To measure the salinity a drop sample was taken with a pipette from different places and depths in the tanks in order to check the uniformity of the salinity throughout the water volume after salt dissolving. The water volumes, the amount of salt at each step and the calculations of the corresponding change in the salinity for all experiments are summarized in Table 7.2. In the case of bubble clouds experiment the salt added into the receiving tank was more than calculated (680 g instead 534 g) in order to compensate for theowering of the salinity when the less salty water left in the hose from the previous measurement was added. The next measurement started when the salinities in all

Table 7.2

Experiment # short description	Water mass kg	Salt added at a step g	Salinity change at a step $^{o}/_{oo}$ (g kg^{-1})
Experiments 1 & 2 single bubble big tank, filtered water	127.1065	600	4.69
Experiment 3 single bubble small tank, distilled water	24.25	120	4.95
Experiment 4 bubble clouds receiving tank supply tank	88.93 130.33	534 780	6.00 5.98

volumes (the receiving tank, the supply tank, and the hose), were equalized. In Figure 7.2a the salt mass added at a step and the corresponding change in the salinity for the three experiments on a single bubble are plotted. In Figure 7.2b the same parameters for the receiving and supply tank in the bubble clouds experiments are given.

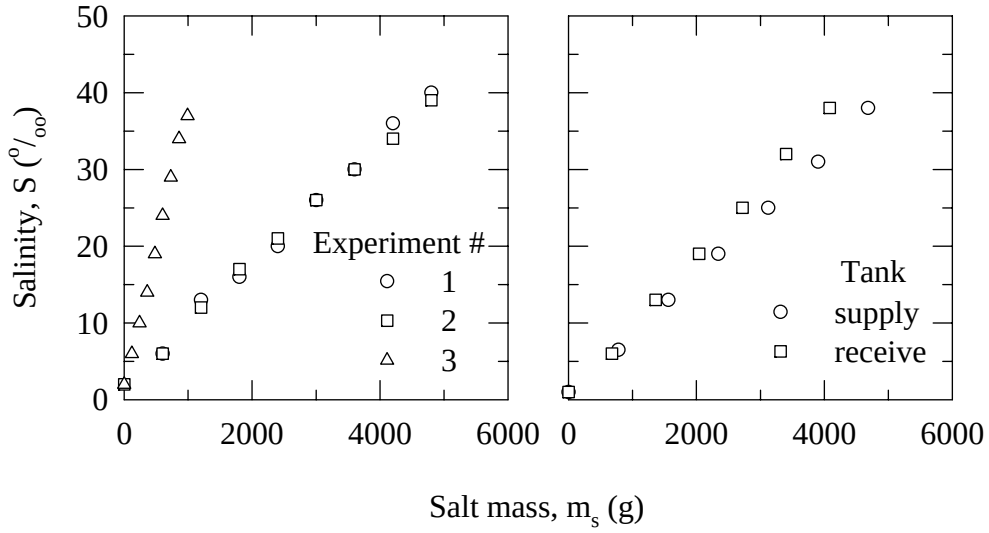

Figure 7. 2 Salinity of the water obtained by adding salt: a) for the three experiments on a single bubble; b) for the bubble clouds experiment.

The influence of sea water composition on surface tension was considered in §3.3.2 in details: the surface tension of saline water is less than that of fresh water. This is generally the reason why the sea water breaks more readily into bubbles, and in particularly bubbles with smaller diameters to be generated. In addition, the coalescence between bubbles is prevented by the organic film accumulated quickly on the bubble wallsand the ionic nature of the sea water, so that the tendency of preserving the small bubble sizes is strong. As was already noted (see §2.2.2), bubbles with different diameters have different rise speeds, hence different residence times in the water column before surfacing and bursting. Therefore, the surface tension was the most important parameter to be controlled during the experiment. The surface tension of a water sample of 150 ml was measured with a tensiometer each time when the salinity was changed in the volumes for all experiments. Up to ten readings of the weight change were taken for statistically sound results in the single bubble experiments. For each reading the water sample was changed and the platinum plate heated (to remove the contaminants) and tempered. For the bubble clouds experiment the surface tension in the receiving tank only was controlled and one weight reading was made.

As for most inorganic solutes in water (Figure 7.3), the addition of salt to pure water slightly raises the surface tension. This effect, however, is easily masked by the strong downward trend of γ if even a small amount of organic compounds are present in the sample (Scott, 1975; Rosen, 1978; Handbook of chemistry and physics, 1986-1987, p. F-31) . The later fact created a lot of difficulties during the experiments. The trends of surface tension with salinity for water with different quality are compared in

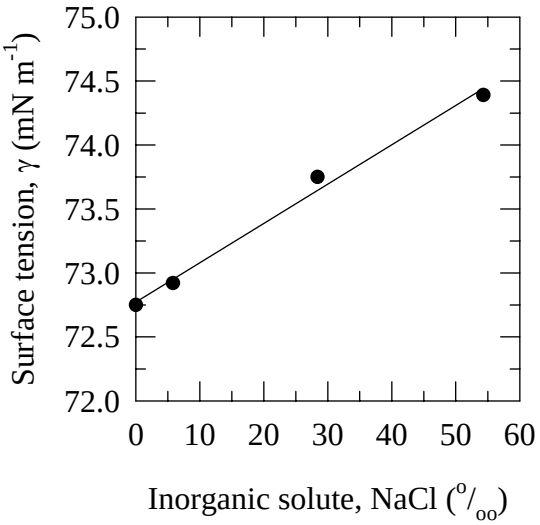

Figure 7.3 Surface tension dependence on NaCl concentration (the data are from the Handbook of chemistry and physics, 1986 - 1987, p. F-31) .

Figure 7.4. In the figure panels a and b show that indeed the salt increases the surface tension when added to distilled or well filtered water. Moreover, the purer the water the stronger the increase as the comparison between the trends for distilled (a) and well filtered (b) waters show. In panels c and d the masking of the salt effect by the presence of organic compounds in tap and not well filtered water is confirmed. As the tap water contains more organic additives, their influence on the surface tension is much better expressed in panel c than for not well filtered water in panel d. The surface tension values in Figure 7.4 were obtained for a small water volume (150 ml), for which the water quality was easy to keep. As discussed in § 2.2.2, to achieve purity in the experimental system is not an easy task, especially for a large water volume as that used in the experiment with the distilled water described here (water mass of 24.25 kg) . Indeed, despite all precautionary efforts

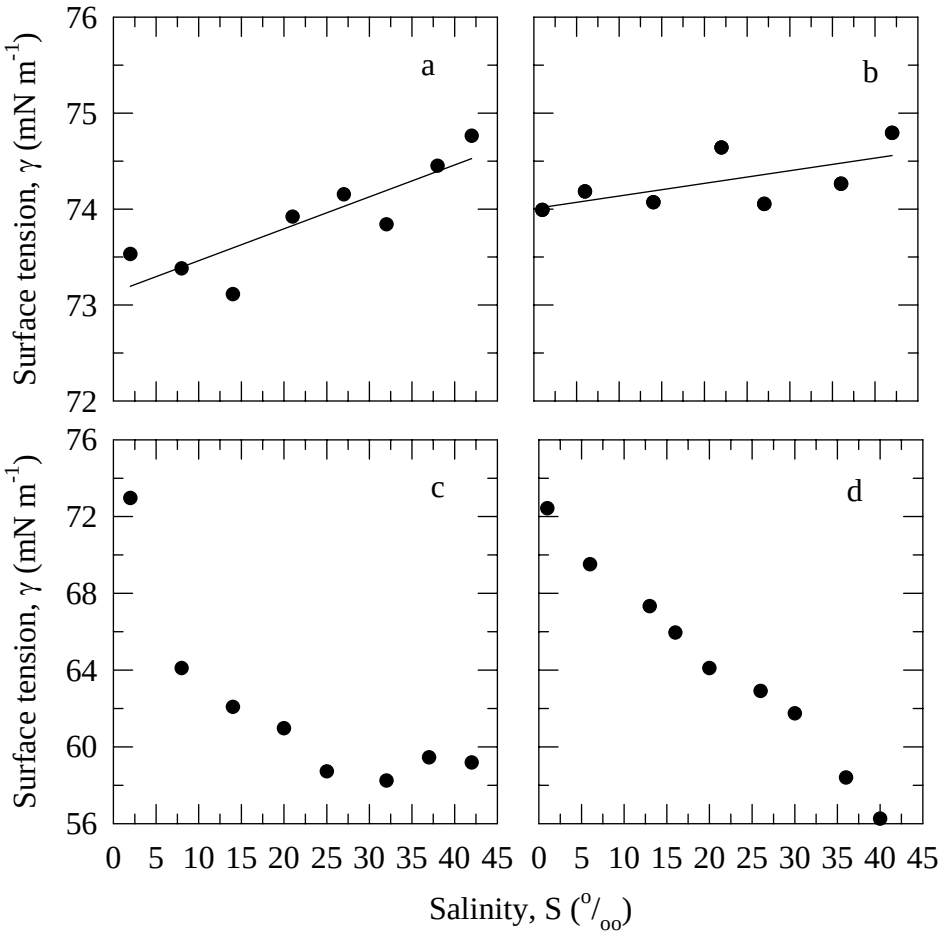

Figure 7. 4 Trend of the surface tension vs. salinity for water with different quality: a) distilled; b) well filtered; c) tap; d) not well filtered.

it was hard to keep the water quality throughout the experiment. Nevertheless, the pure effect of salinity on the surface tension and bubble characteristics was revealed though not perfectly.

It was necessary to control the water temperature since the temperature affects the surface tension, while it was desirable to cause surface tension changes only by changing salinity. Generally, the surface tension decreases with temperature rising. A theoretical

calculations of this effect at different salinities, S $^{o}/_{oo}$, and temperatures, T^{o}C, are made using the empirical equation (Brahtz, 1968):

$$\gamma = 75.64 - 0.144T + 0.0399S$$

and compared in Figure 7.5a. The surface tension values for fresh water (S = 0 $^{o}/_{oo}$) at different temperatures calculated with this equation coincide well with the values tabulated in the Handbook of chemistry and physics (1986-1987), Table 7.3. During the experiments, water temperature changed slightly with the diurnal cycle (some experiments lasted a few days; recall the first two experiments on a single bubble described in §7.2.1) and mostly because of the lighting used for the video records. Strict usage of the lighting only for the period of recording yielded to almost no variations of the water temperature. For most measurements the water temperature fluctuations during procedures at a given salinity were 0.2 - 0.3°C, while those between different salinity steps seldom exceed 0.5°C. It is revealed from Figure 7.5b that a temperature rise of 0.5^{o}C would cause a

Table 7.3

Temperature, T (^{o}C)	Surface tension, γ (mN m^{-1}) calculated values	Surface tension, γ (mN m^{-1}) tabulated values
0	75.64	75.6
5	74.92	74.9
10	74.20	74.22
15	73.48	73.49
20	72.76	72.75
25	72.04	71.97
30	71.32	71.18

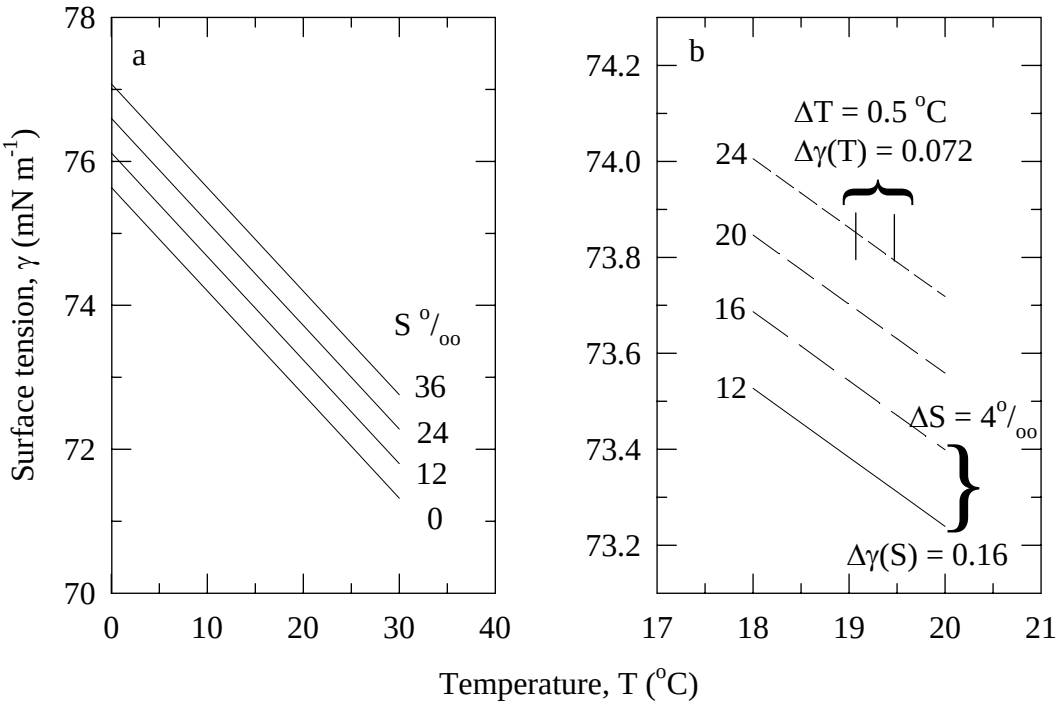

Figure 7. 5 Surface tension dependence on temperature: a) values calculated with an empirical equation; b) changes with a small step ($\Delta T = 0.5°C$) .

decrease of the surface tension by 0.072 mN m^{-1} at a given salinity, while an increase of salinity with $4^{o}/_{oo}$ would increase it by 0.16 mN m^{-1}. Only in two cases were the temperature variations for consecutive salinity steps larger, up to 1.5°C, however the surface tension changes at these moments were higher than that caused by temperature alone. Thus, it is fair to say that the temperature effect on the surface tension was eliminated, and whatever changes of surface tension were observed were caused from salinity difference provided that organic compounds were removed or kept constant. The values of the controlled parameters for all experiments are summarized in Table 7.4.

Table 7.4

Single bubble experiments											
Experiment 1				Experiment 2				Experiment 3			
S $^{o}/_{oo}$	γ mN m^{-1}	σ_{γ} mN m^{-1}	T ^{o}C	S $^{o}/_{oo}$	γ mN m^{-1}	σ_{γ} mN m^{-1}	T ^{o}C	S $^{o}/_{oo}$	γ mN m^{-1}	σ_{γ} mN m^{-1}	T ^{o}C
1	72.43	1.11	18.6	2	66.92	1.92	17.4	2	60.87	4.08	19.7
6	69.51	2.91	20.1	6	67.14	2.03	18.2	6	66.15	4.75	19.9
13	67.33	1.28	19.5	12	65.66	3.95	17.10	10	71.19	2.62	20.1
16	65.94	3.65	19.8	17	62.83	6.08	18.1	14	70.47	4.00	20.3
20	64.09	5.92	19.2	21	62.21	4.24	18.1	19	74.79	0.40	20.3
26	69.28	6.21	19.0	26	63.49	3.66	18.2	24	72.98	3.49	20.5
30	61.73	6.22	19.1	30	61.27	3.82	18.5	29	70.78	5.38	20.2
36	58.40	3.82	19.0	34	58.21	5.15	18.7	34	71.74	5.00	20.1
40	63.5	5.25	19.0	39	54.28	5.08	18.7	37	69.49	11.97	20.5

Bubble clouds experiment				
Supply tank		Receiving tank		
$S^{o}/_{oo}$	T°C	$S^{o}/_{oo}$	γ mN m^{-1}	T°C
1	17.4	1	73.08	17.4
6.5	17.3	6	74.22	17.4
13	17.3	13	74.12	17.4
19	17.3	19	72.39	17.3
25	17.3	25	73.44	17.3
31	17.3	32	73.76	17.2
38	17.2	38	69.51	17.2

7.3 Data Processing

7.3.1 Parameters to be Measured

The parameters necessary to be measured in a single bubble experiments were bubble diameter, d (mm), bubble rise velocity, V_r (cm s^{-1}), and bubble surface lifetime, t (s) . In the bubble clouds experiment those were the number of bubbles generated within the cloud, the bubble cloud shape and depth of penetration, and the void fraction of the cloud (the volume occupied by the air bubbles in the cloud volume) .

7.3.2 Procedure

7.3.2.1 Single Bubble Data

The bubble rise velocity (V_r) and bubble surface lifetime (t) were determined from direct observations and video records.

From the direct observations the rise velocity was found by measuring the reference distance and the time for traveling along it averaged for all 15 time readings. The large variance of this timing due to error from hand reaction was unavoidable, but rectified with much more accurate results from the video records.

The surface lifetime was found by averaging the 15 time readings made for the floating bubbles. The variance in this case was even larger than that for rise velocity. The reason was not only the hand reaction error, but also in the of observation of both, almost immediately bursting bubbles ($t < 1$ s) and long lasting bubbles (up to 20 s).

The bubble rise velocity (V_r) and bubble diameter (d) were determined from the side view video records; bubble surface lifetime (t) – from video records of floating bubbles from above. To determine the bubble diameter up to 30 frames with bubble images were digitized for each salinity step. As it was anticipated from the predicted diameters (Table 7.1) and discussed in §2.2.3, the images clearly documented the ellipsoidal shape of the bubbles. Hence, an equivalent diameter was determined using the procedure for this described in 6.3.3.2. Finally, the mean and variance of the series with equivalent diameters were found and reported.

The time for traveling of a reference distance by a bubble was obtained from the side view video records by counting the frames necessary for this trip and using the time interval between the frames (33 ms) . For each salinity this time was determined for 10 bubbles; the repeatability in the number of frames for traveling the reference distance was remarkable. Using the averaged time for these 10 bubbles and the reference distance the rise velocity was calculated.

The bubble surface lifetime was derived from the top view video records either by counting the number of frames during which a bubble lies on the surface or by using the time recorded from the camera timer. When bubbles coalesced, they were excluded from the consideration. Data were extracted for 30 to 50 bubbles. Again, as for the direct observation, a wide range of variations for surface lifetime were observed (hand reaction error was excluded) . Therefore, it was more pertinent to present the distribution of these values than to find their average. In addition, the average values

with their variances were derived in order to get the general trend of surface lifetime changes at various salinities.

7.3.2.2 Bubble Cloud Data

For each salinity step a sequence of 30 images of bubble clouds was organized by digitizing each 60-th frame, time interval of 2 s, in the 1-minute video records. The digitizing window was 664 pxl x 192 pxl, which represented a part of the whole field of view (see §7.2.2) with sizes 19.65 cm x 13.4 cm.

9999 The processing procedure for the bubble clouds shape and depth of penetration followed several steps illustrated in Figure 7.6 for salinity S = $13^{o}/_{oo}$. First, from the raw images (Figure 7.6a) an initial field of view without bubble clouds was subtracted in order to remove the background lighting: images became well contrasted (Figure 7.6b). Then, all 30 images of bubble clouds were averaged and the silhouette of the cloud revealed in the resultant image (Figure 7.6c). Next, edge detection applied to this image visualized well the cloud boundary (Figure 7.6d). Finally, several points of this boundary were extracted for further graphing.

The number of bubbles within a bubble cloud was counted with a command available in the software. The very big blobs resulting from bubble coalescence, especially for fresh and low-saline water, were excluded from the counting by introducing restriction on the size of the blobs to be counted. As the relative changes in the number of bubbles at

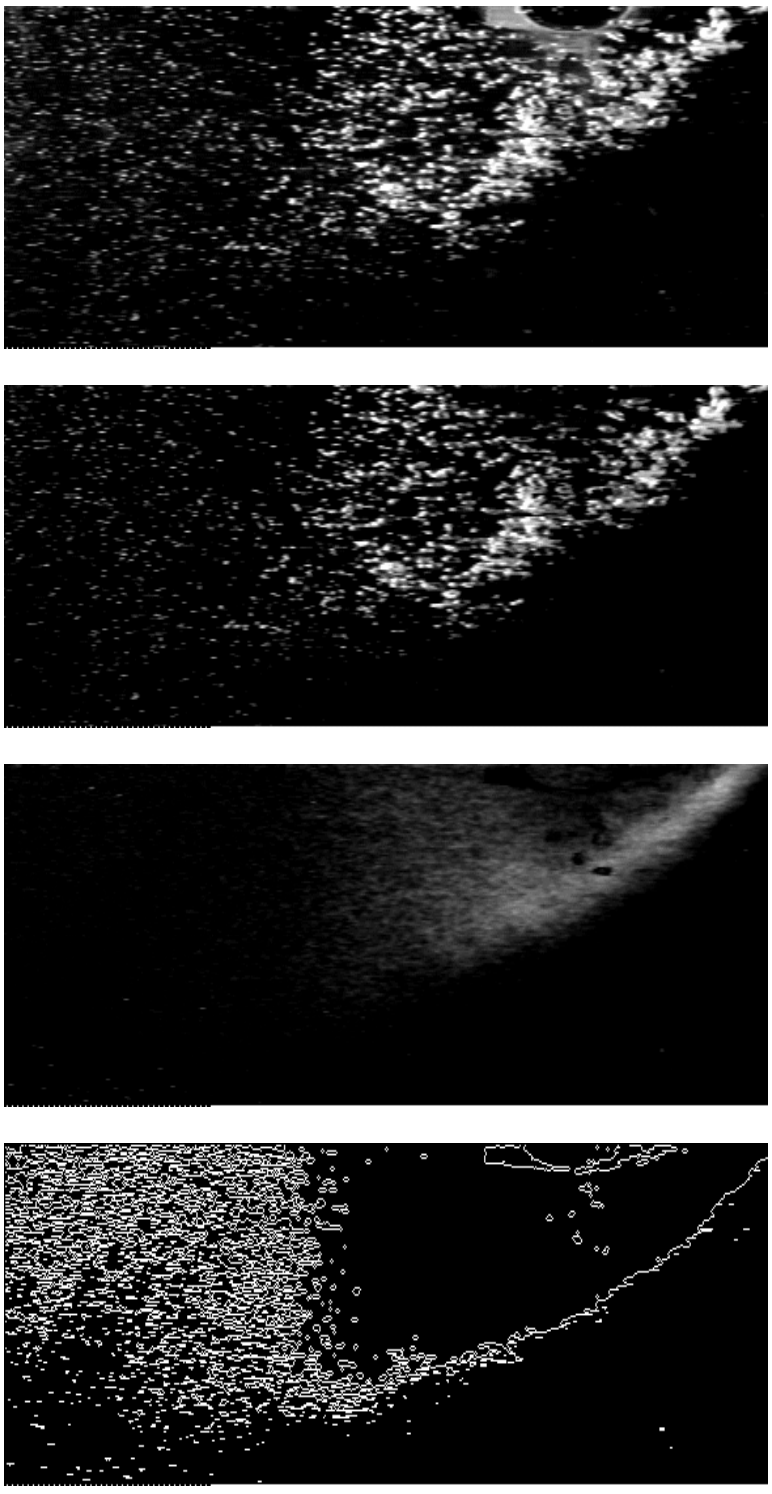

Figure 7.6 Processing steps for bubble cloud shape and depth of penetration: a) raw image; b) image with subtracted background; c) bubble cloud silhouette (result of averaging of 30 clouds); d) edge detection reveals the cloud boundary.

various salinities is of interest rather the absolute number, the underestimation due to these restrictions is not important.

The void fraction was calculated as in the experiments on bubble cloud characteristics: the ratio of the bright pixels (representing air) counted within the cloud volume, framed with a freehand drawn boundary, to the all pixels (representing air-water mixture) in the same frame. The criterion for separation of the bright pixels from the "mixture" pixels was an intensity threshold. This procedure was applied for all 30 images at each salinity and data were saved in a file for further calculations and plotting. All described procedures were facilitated by using macros.

7.4 Results and Discussion

7.4.1 Results on a Single Bubble

Images of a bubble rising through the water column at seven consecutive moments (Δt = 33 ms) are overlapped to reveal its motion in Figure 7.7. The bubble is with an ellipsoidal shape, with the longer axis horizontal, and moves upward on zigzag path – features predicted (Soo, 1967; Clift, 1978) and correctly observed here. This fact does not change with increasing the water salinity. The bubble diameter constancy over the entire range of salinity is illustrated in Figure 7.8. The salt concentration does not influence the bubble size directly. The salinity changes the ionic strength of the water and hence the rate of coalescence between neighboring bubbles, which eventually brings

different time evolution of the bubble size distributions in waters from different sites, for instance in the open ocean, coastal zone or at the river outlet.

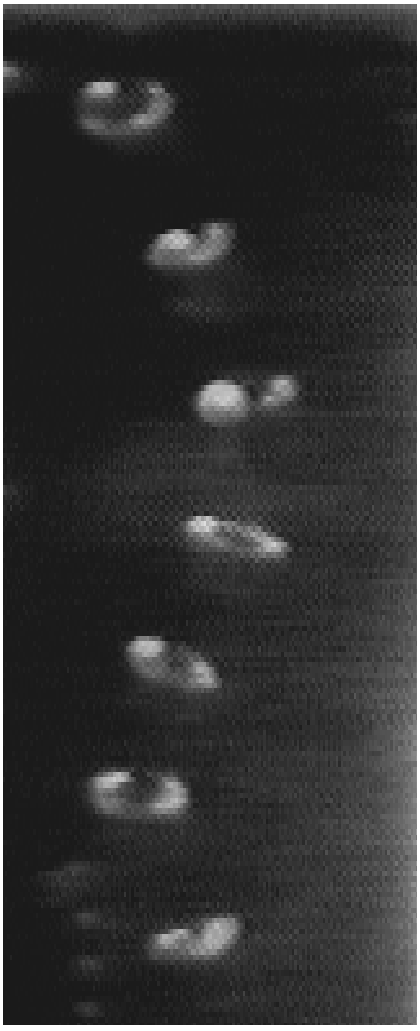

Figure 7. 7 A single bubble in seven consecutive moments (Δt = 33 ms) on its helical path.

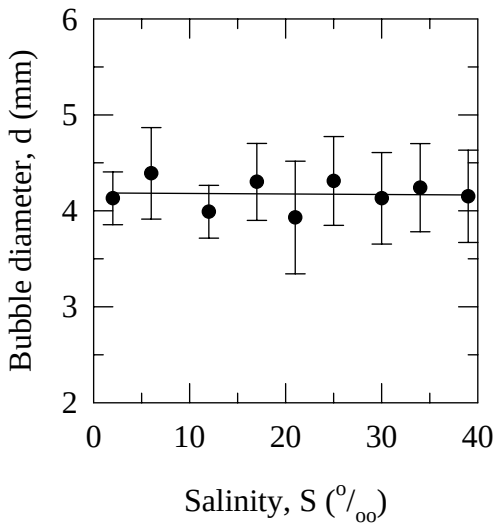

Figure 7. 8 Bubble diameter remains constant over the entire salinity range. The data are for experiment 2.

The results on bubble rise velocity V_r obtained from the video records for the three experiments are summarized in Figure 7.9. For experiments 1 and 3 the rise velocity associated with a certain bubble diameter (shown in the figure) does not change more than its experimental variance with increasing the salinity. There is a hint for a peak in experiment 2, but the wide variances do not allow to say confidently if this is the peak discussed in §2.7.1 or an experimental scattering. The water quality (announced in the figure), and hence the different trends of the surface tension, does not influence the rise velocity either. It was stated before (§2.7.1) that the surface active materials have strongest influence on the bubbles in the ellipsoidal regime. The results in Figure 7.9 are for bubbles of this kind and show very little effect of the salinity on the rise velocity once a bubble with a given size is generated. Consequently, it is almost certainly expected that the rise velocity of bubbles with other diameters, for example those typical for the ocean

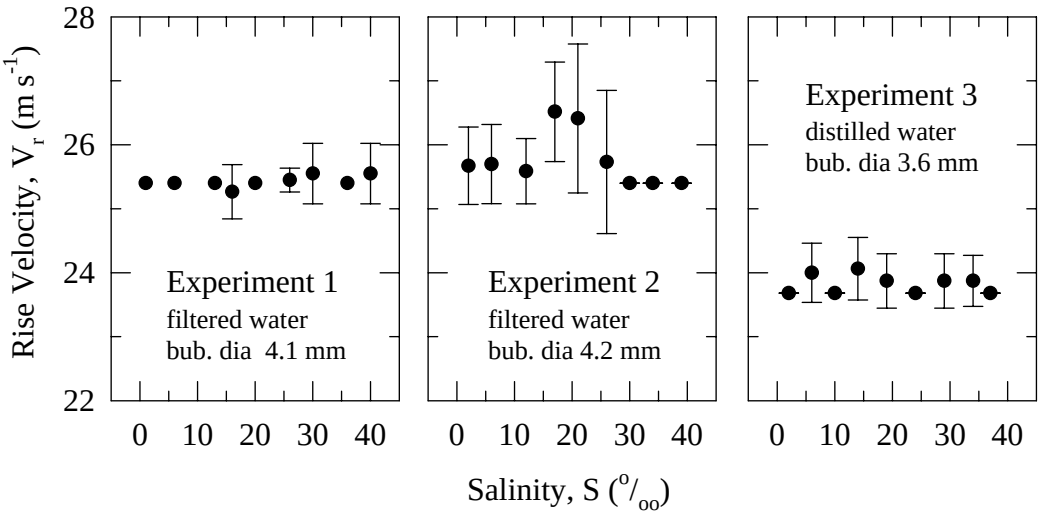

Figure 7.9 Bubble rise velocity vs. salinity. (Experiments 1, 2, and 3, video records.)

bubble population, will not exhibit any particular trend with salinity variations. Of course, the absolute value of the rise velocity would be different for the different diameters. Results on the rise velocity obtained from direct observations during experiment 1 are compared with those from the video records in Figure 7.10. The wide variance of the

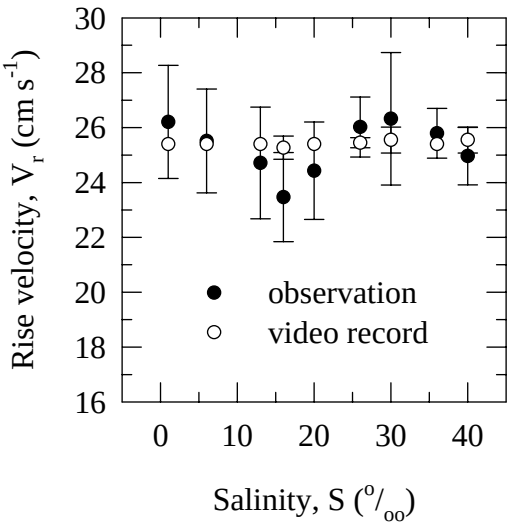

Figure 7. 10 Comparison of the results on bubble rise velocity obtained from observations and video records (experiment 1) .

observational results points to the measurement error (hand reaction) rather than to some velocity changes with salinity. The velocities for three different bubble diameters, all of them in the ellipsoidal regime, are compared in Figure 7.11. The smallest diameter has the highest velocity as these bubbles belong to the intermediate region where the velocity falls with bubble diameter increasing (recall Figure 2.4) .

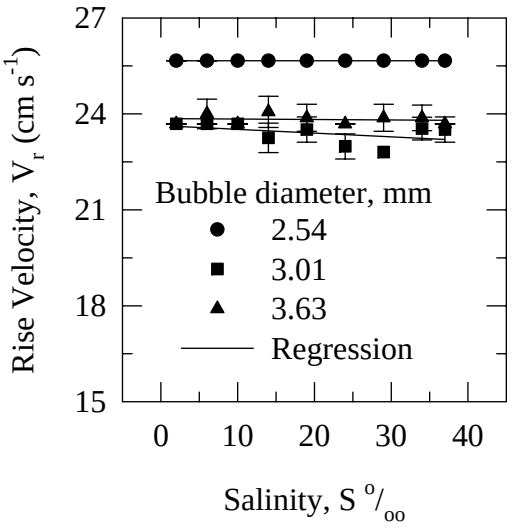

Figure 7. 11 Rise velocity for different bubble sizes. (Experiment 3, video records.)

Images of bubbles floating on the water surface before their bursting are pictured in Figure 7.12. With the flow rate adjusted the bubbles rarely overlapped on one and the same place in fresh water and in diluted solutions. They either burst before the next bubble popped, or drifted away from the place of surfacing. However, when a bubble lingered until the next one appeared in a close vicinity, immediate attraction and coalescence occurred. With increasing the salt concentration the bubble surface lifetime was prolonged, and then in some occasions the bubbles simultaneously existing on the

Figure 7. 12 Bubbles floating on the water surface before bursting.

surface attached to each other and persisted in a cluster for a while until they finally coalesced or burst.

Considerable variance of the surface lifetime values, as it was mentioned earlier (§7.3.2.1), was registered. Therefore, it seems proper to consider the distribution of these varying data over a time range 0 - 20 s with a bin of 1 s. Probability density functions from direct observation and from video records in experiment 2 are given in Figures 7.13 and 7.14, respectively. It is seen from both approaches (observations and video records) that in fresh water ($2^{o}/_{oo}$) the surface lifetime values are concentrated in the range from less than a second to about 5 s with typical values 1 s. With increasing the salinity up to $12^{o}/_{oo}$ the range of possible surface lifetime values broadens to 12 - 18 s. Further increase of the salinity (17 - $30^{o}/_{oo}$) confines the values in the range 10 - 12 s, until at highest salt concentrations (34 and $39^{o}/_{oo}$) most of the bubbles live less than a second and at most 5 s. Interesting observation is that only with a few exceptions a large fraction of the bubbles have surface life less than 1 s at most 2 second for all salinities. In figure 7.15 the results

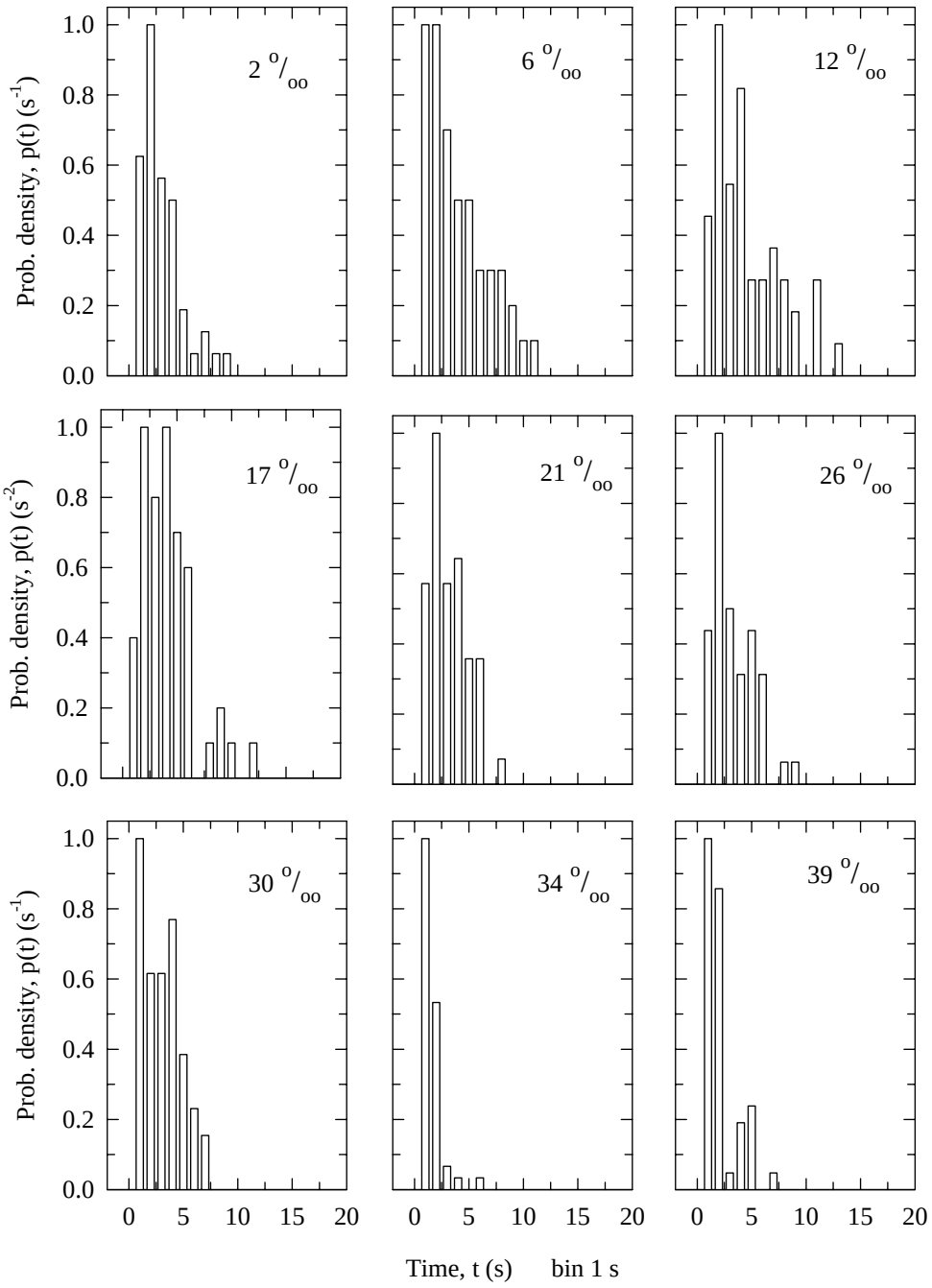

Figure 7.13 Distributions of the bubble surface lifetime values with varying salinity concentrations. (Experiment 2, observations.)

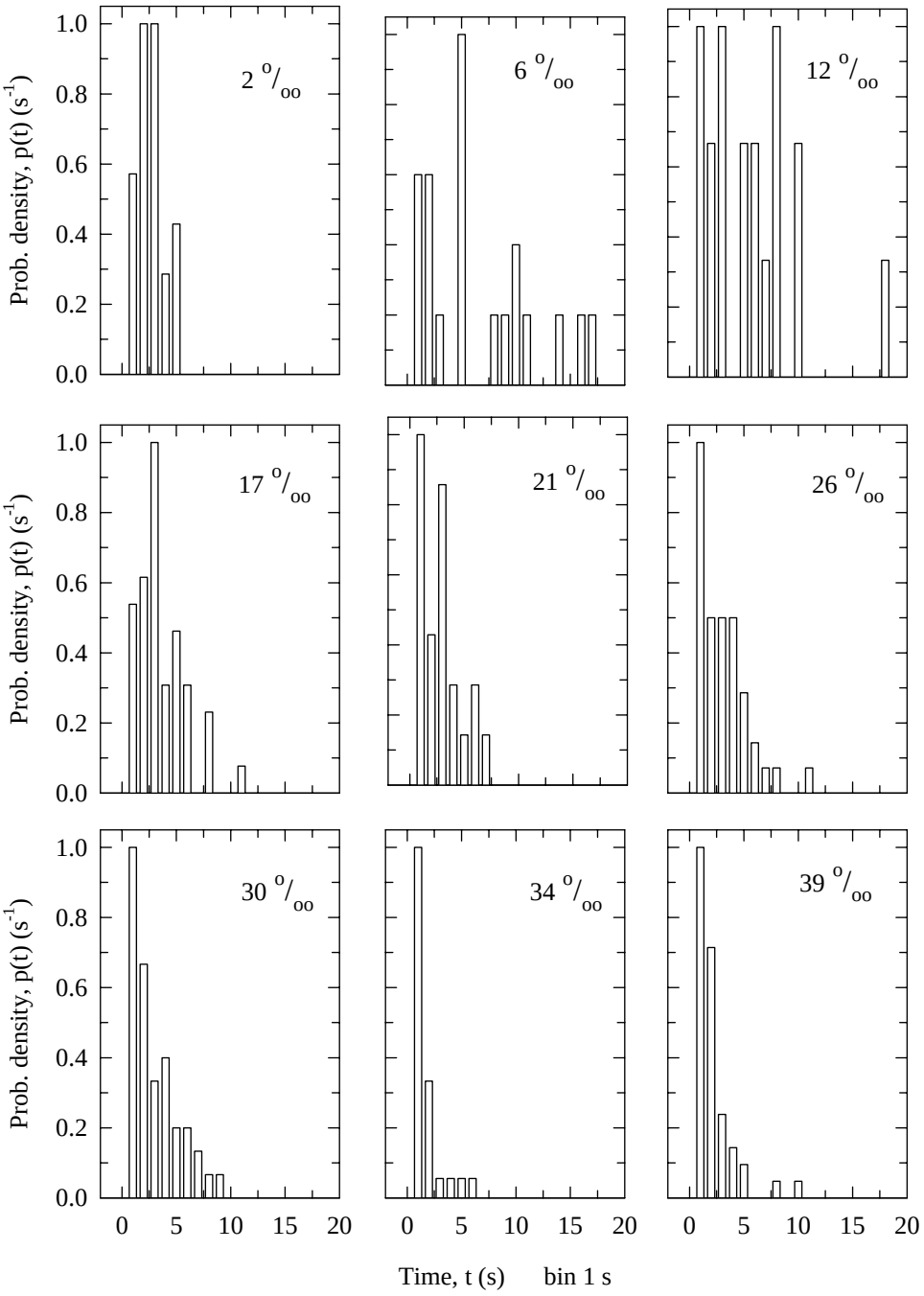

Figure 7.14 Distributions of the bubble surface lifetime values with varying salinity concentrations. (Experiment 2, video records.)

from observations and video records clearly delineates the general trend of bubble surface lifetime stabilization for some narrow salinity range despite the wide variances. In the light of the discussion in §2.7.2, the increase in bubble longevity on the surface is a result of the increased elasticity of the surface film acquired from the organic in the

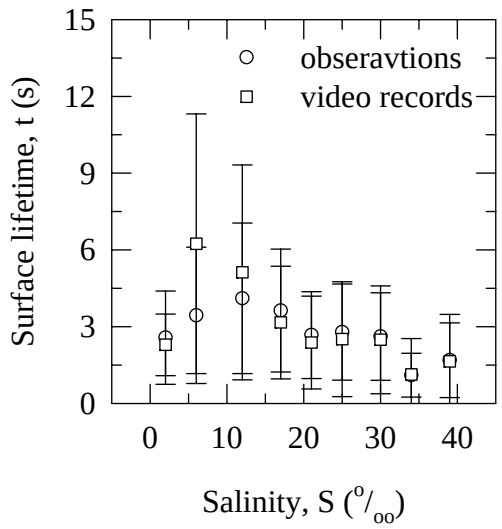

Figure 7.15 Comparison of the observed and video recorded results on surface lifetime.

water. This effect is obviously additionally facilitated and enhanced by the salinity content. The processes taking place during the three experiments (1, 2 and 3) can be traced in Figure 7.16. In the figure the upper panels show the surface tension behavior, related to the film elasticity, and the lower panels give the observational results of the corresponding bubble surface lifetime versus salinity. Although the water for experiments 1 and 2 (panels a and b) is filtered, some small organic content remains and this reduces the surface tension. Assuming that the concentration of the organic additives is constant for a given

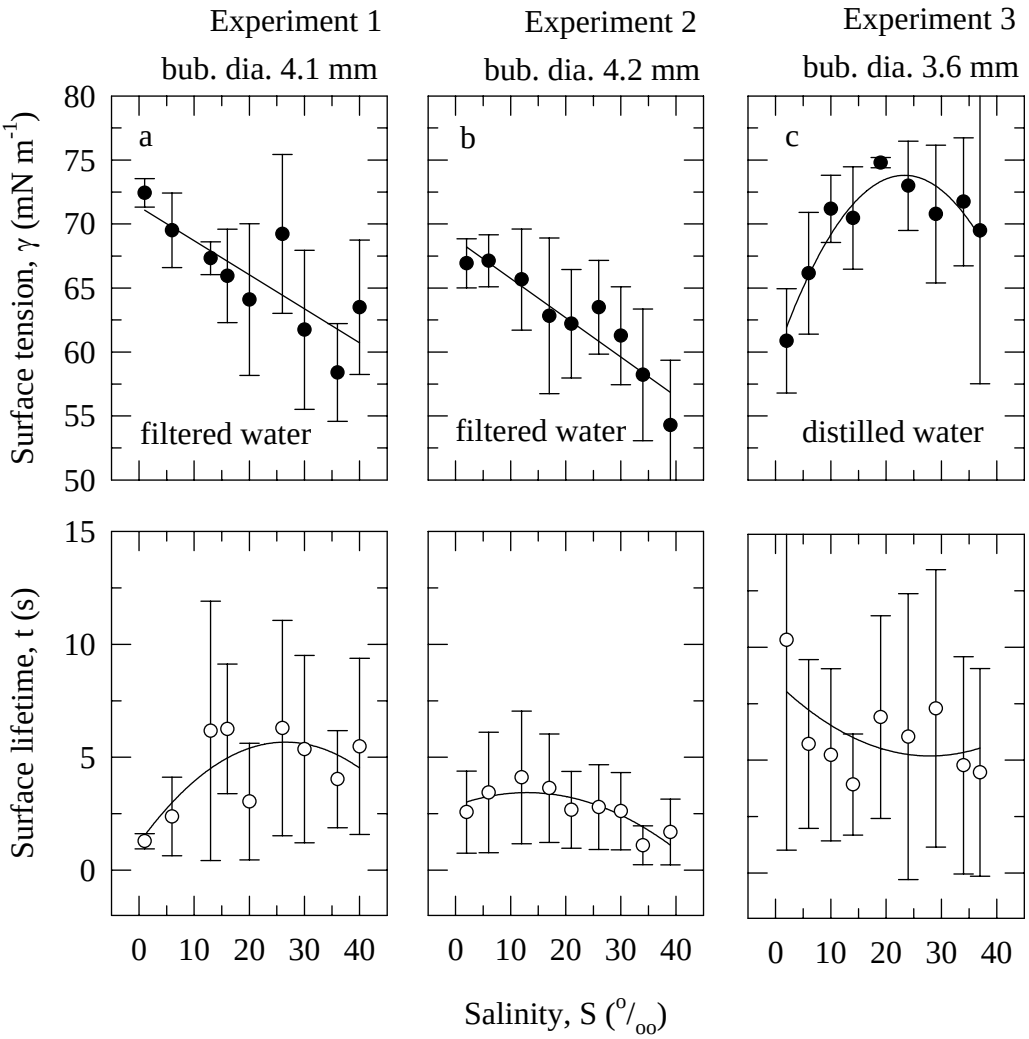

Figure 7. 16 Surface tension (upper panels) and surface lifetime (lower panels) vs. salinity. (Experiments 1, 2, and 3.) The solid lines are best polynomial fit.

experiment, the surface tension should stay at this decreased value. However, with increasing salinity surface tension values exhibit a steadily decreasing trend. This effectcan be explained with the fact that the salt concentration enhances the adsorption of the organic film on the surfaces (2.7.2), and as a result the surface tension continuously diminishes as if the concentration of the organic matter is increased. The Gibbs effect

(2.7.2) then arises and the film elasticity would reach some maximum value (Figure 2.8) with a net effect of stabilizing the bubble surface lifetime. This stabilization is maximum for salinities in the range 10 - 20$^{o}/_{oo}$. After that the high salinity values (25 - 39$^{o}/_{oo}$) help the surface film molecules to pack densely, the film elasticity decreases and as a result the bubble surface lifetime decreases too or behave uncertainly. Only in the case when organic compounds are isolated (experiment 3 with distilled water) surface tension values increase with salinity, and the surface lifetime of the bubble decreases (Figure 7.16c) . The pure effect of salt to diminish the surface tension repeats for all three bubbles diameters generated during the experiment 3, Figure 7.17. The wide variances can be explained with an effect discussed by Garrett (1967) . When a bubble floats on the water surface and bursts, the surface film that otherwise stabilizes the bubbles is perturbed for some while. Though it can recover after only a few seconds, if a new bubble appears on the surface at

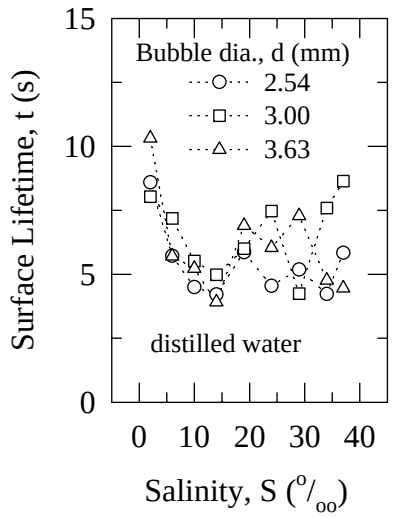

Figure 7.17 Surface lifetime of bubbles with different diameters vs. salinity. (Experiment 3, observations.)

this moment, its lifetime will be determined by the new conditions: the surface might be clean for a short interval and then the bubble will live less than a second; or the film might be thin and not sufficiently elastic to stabilize the bubble.

The increase of bubble surface lifetime accounts for the well known whitish appearance of the coastal zone. This has implications for the remote sensing techniques as the scattering and reflection from foam patches is quite different from water without foam (Koepke, 1986; Frouin, 1996) . The prolonged residence of the bubbles at the surface before bursting makes the coalescence more likely, and hence leads to an increase of bubble size. As the number and size of the sea aerosols produced by bursting bubbles depend on the parent bubble size, the ultimate result would be an increased sea aerosol production. For example, a bubble of 3 mm diameter on the surface would produce 3 jet and 9 film drops according to figure 5 of Resch and Afeti (1991), or 12 drops overall. If as a result of longer life, coalescence takes place and bubble size increases to 6 mm, this new bubble would produce 1 jet and 30 film drops (Resch and Afeti, (1991), or 31 drops overall, which means that the aerosol production rate increases 2.6 times.

7.4.2 Results on Bubble Clouds

Images of bubble clouds in fresh water and water with salinity 13, 25 and $38^{o}/_{oo}$ are shown in Figure 7.18. The bubble cloud in fresh water (the top panel in the figure) is clearly separated in two parts as Hwang et al. (1991) observed: a part withmany large bubbles near to the source and another with a few small bubbles. With

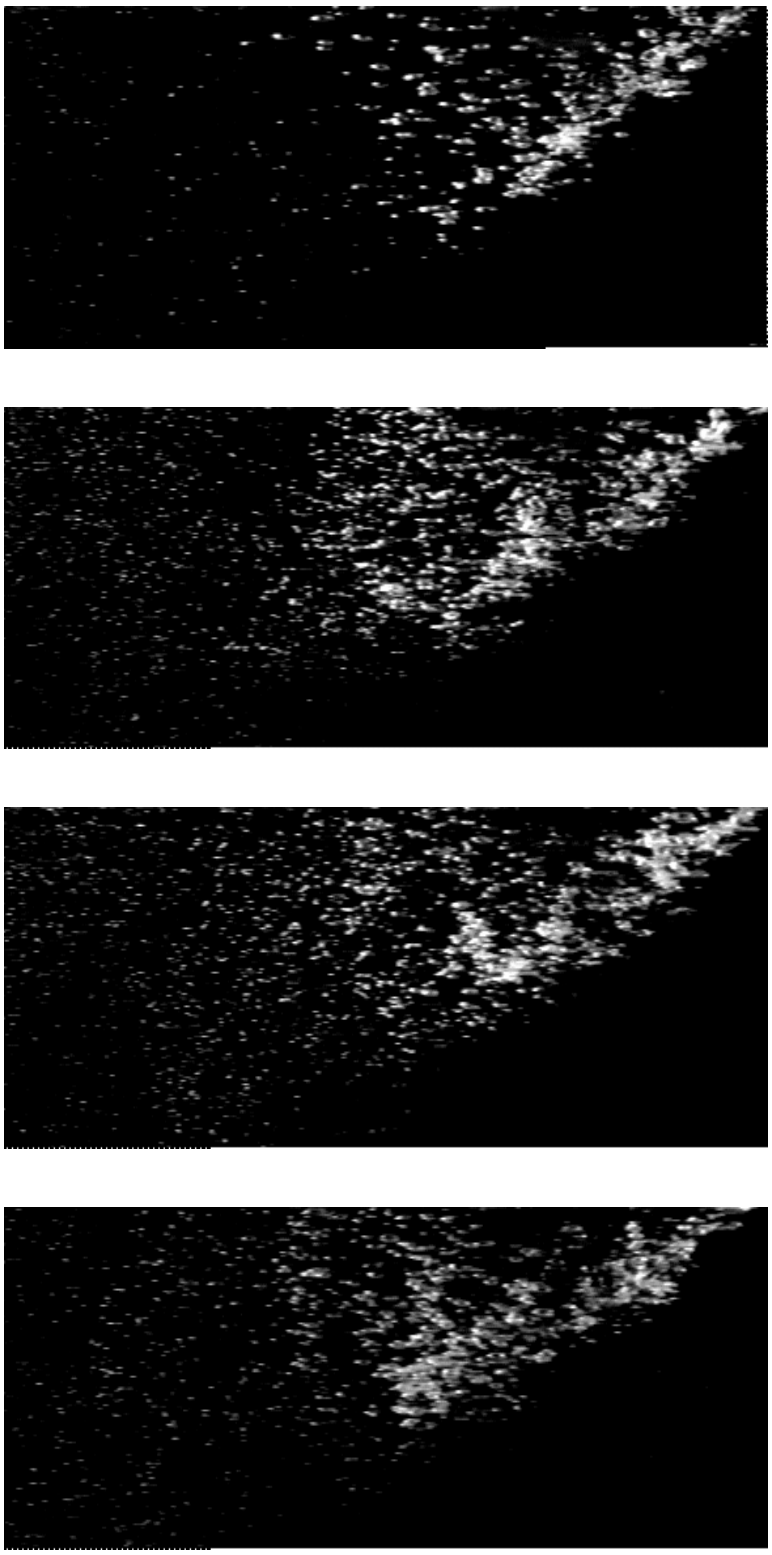

Figure 7. 18 Bubble clouds in fresh and saline water (from top to bottom S = 2, 13, 25, and $38^{o}/_{oo}$) .

increasing salinity of the water the number of the small bubbles increases significantly, as was also observed by Scott (1975). Quantitative result of this effect is plotted in Figure 7.19. The number of bubbles within the cloud, normalized with the maximum observed value, increases with increasing the salinity and passes through a maximum in the range of 13 - 25$^{o}/_{oo}$, then the number of bubbles decreases again. Looking back at Figure 7.18 another feature becomes obvious: the gradual separation of the bubbles by size. From right to left bubble size evidently decreases and while the large bubbles are quick to go up and their penetration depth is low, the small bubbles travel deeper and start their rise at greater depths. This behavior forms the plume observed here, and also the plumes forming the clouds generated by wind waves and extensively discussed in Chapter 6. The shape of the plume generally does not change with the salinity. Only its lowest point goes deeper as smaller bubbles are generated. Using the procedure described in §7.3.2.2 and

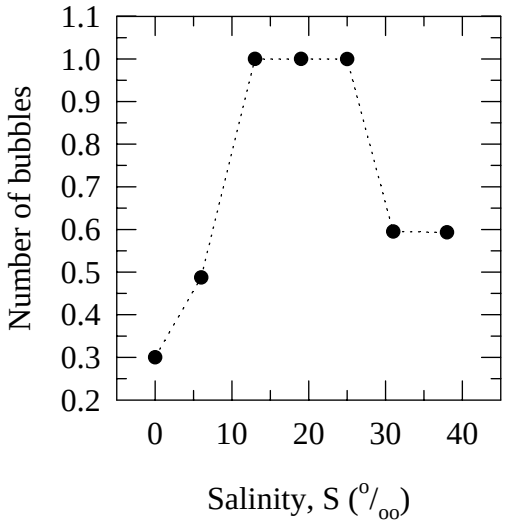

Figure 7. 19 Number of bubbles within the bubble cloud, normalized with the maximum number of bubbles, vs. salinity.

presented in Figure 7.6, the contours of the bubble clouds at different salinities are extracted and piled together in Figure 7.20a. It is seen that indeed the cloud boundaries do not change with salinity more than the variance, Figure 7.20b. The penetration depth for the large bubbles is around 2 cm for all salinities, while for the small bubbles it can go far beyond 13 cm (the resolution of the video camera does not allow the observation of the smallest bubbles, hence the deepest point of the plume) .

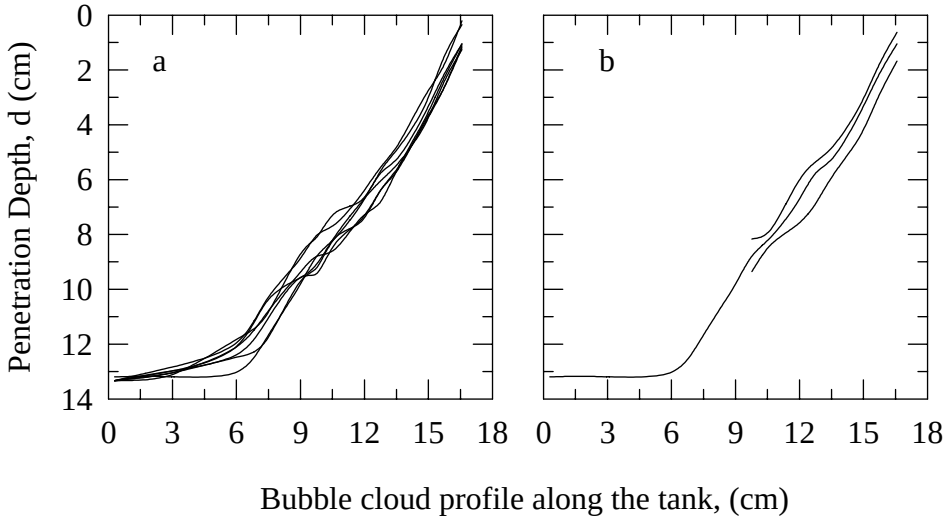

Figure 7.20 Bubble cloud shape and penetration depth vs. salinity: a) the bubble cloud contours for different salinities (2 - 38$^{o}/_{oo}$); b) bubble cloud contour only for fresh water together with the variance.

The void fraction follows closely the trend established by the number of bubbles, Figure 7.21. Again, with increasing the water salinity the void fraction increases to a maximum of 40% for 20 - 25$^{o}/_{oo}$ and then decreases to around 30%. The maximum values of the void fraction around salinity 15 - 20$^{o}/_{oo}$ implies that relative to

open ocean salinities the gas exchange will be enhanced in coastal area due to the production of much

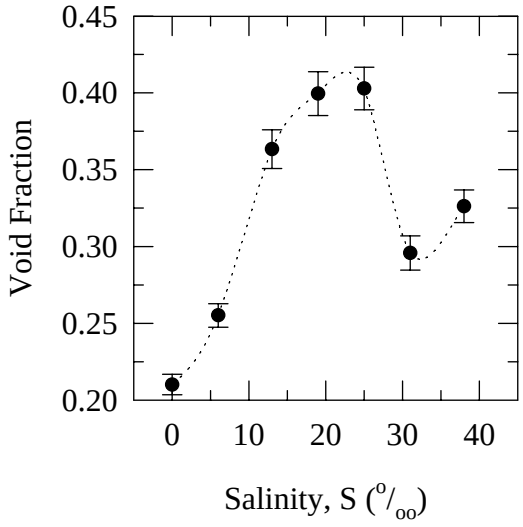

Figure 7. 21 Bubble cloud void fraction vs. salinity.

more small bubbles, hence increased area for gas exchange. In the open ocean, where 75% of the water has salinity in the range of 34 -35$^{o}/_{oo}$, salinity plays a diminished role as regards gas exchange.

7.5 Summary

This chapter deals with the experiments for the salinity influence on bubble and bubble clouds characteristics. Video images of single bubbles, generated with a capillary, and bubble clouds, simulated with a water jet, were analyzed. Salinity of the water was changed from fresh to 40$^{o}/_{oo}$ by adding salt. Surface tension and temperature were controlled. Results on changes of diameters, rise velocity and surface

lifetime of single bubbles, and number of bubbles within, shape and void fraction of bubble clouds with salinity were obtained.

The salinity of the water does not change the diameter of the bubbles. As expected, the rise velocity does not change with the salt concentration either. The salinity influence these bubble characteristics indirectly through changing the coalescence rate between bubbles. Surface lifetime of floating bubbles increases in salt solutions containing organic material. A peak of their longevity appears for salinity in the range 10 - $20^{o}/_{oo}$. The effect of salt itself, in absence of organic additives, is to decrease the bubble surface lifetime. This effects are repeated for different bubble diameters.

Bubble clouds in water with various salinities do not change their shape. Only their lowest point goes deeper as smaller bubble which penetrate deeper are formed. The number of bubbles within the cloud increases with salinity and exhibits a peak for the range 12 - $25^{o}/_{oo}$. Further increase of the salt concentration decreases the number of bubbles again. The void fraction of the cloud follows the same trend.